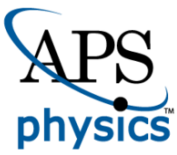

Dynamics and Statics of DNA-Programmable Nanoparticle Self-Assembly and Crystallization

C. Knorowski, S. Burleigh, and A. Travesset

Phys. Rev. Lett. **106**, 215501 — Published 25 May 2011

DOI: 10.1103/PhysRevLett.106.215501

Dynamics and Statics of DNA-Programmable Nanoparticle Self-Assembly and Crystallization

C. Knorowski,[1] S. Burleigh,[2] and A. Travesset[1]

[1] *Department of Physics and Astronomy and Ames Laboratory, Iowa State University, Ames, IA*
[2] *Department of Physics and Astronomy, Louisiana State University, Baton Rouge, LA*

DNA linker mediated self-assembly is emerging as a very general strategy for designing new materials. In this paper, we characterize both the dynamics and thermodynamics of nanoparticle-DNA self-assembly by Molecular Dynamics simulations from a new coarse grained model. We establish the general phase diagram and discuss the stability of a previously overlooked crystalline phase (D-bcc). We also characterize universal properties about the dynamics of crystallization. We point out the connection to f-star polymer systems and discuss the implications for ongoing experiments as well as for the general field of DNA mediated self-assembly.

Programmed self-assembly, i.e. programming components to self-assemble into materials with pre-defined properties, is one of the ultimate goals in materials science. An elegant strategy consisting of attaching complementary DNA strands to components so as to selectively induce their assembly was pioneered more than a decade ago[1, 2], where gold nanoparticles (GNPs) with complementary single stranded DNA (ssDNA) oligomers attached were assembled into larger entities. This approach has also been intensively investigated with micron sized particles[3], where the larger scales provide promising routes for the bottom-up design of metamaterials.

A recent breakthrough has been the programmed self-assembly of GNPs into phases with long range order, such as bcc and fcc crystals [4, 5, 7–9]. With fundamental advances in controlling the chemistry of nucleotides and the placement of ssDNA onto nanoparticles with exquisite precision [10], the main challenges towards a general and predictive framework for programmed self-assembly are the characterization of the ssDNA distributions that will assemble into a given structure or phase and the elucidation of the kinetic or dynamical properties that determine relaxation times and long-lived metastable states. Recent results showing that in general, the functionalization of polymer ends with specific interactions can direct the self-assembly of nanoparticles into many phases[11], provides further evidence for the potential of DNA programmable self-assembly.

The theoretical prediction of the phases from hybridization of spherical colloids was first described by Tkachenko [12], who developed an effective potential that allowed characterization of equilibrium phases. Subsequent studies focused on simpler models amenable to a mean field solution[13]. Coarse grained continuum molecular dynamics simulations have provided some insights into the dynamics and statics of DNA-nanoparticle self-assembly[14]. Recent work [15] has discussed phase diagrams and kinetic effects from refined effective potentials. Yet, most previous studies either rely on simplifying assumptions (two-body potential interactions, assumptions about the minimum of the free energy, mean field, etc..) and/or are inappropriate to elucidate the self-assembly process since they do not include realistic dynamics.

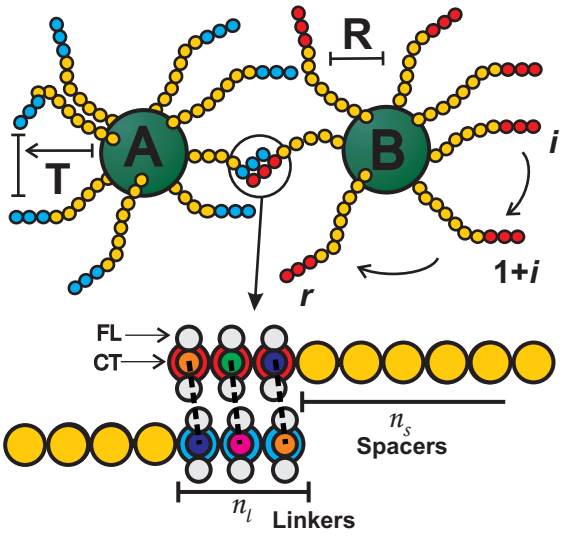

FIG. 1. (color online). Coarse grained Model of ssDNA-GNP. n_s and n_l are the coarse-grained number of spacer and linker beads respectively. r is the number of ssDNA attached to each GNP. R is the radius of a GNP and T is the average end to end distance of the ssDNA. The structure of the ssDNA linker, which allows hybridizations, is modeled with central beads(CT), the complementary basis, and flanking beads(FL).

In this paper, we present a new coarse-grained model for ssDNA-GNPs and simulate it using continuum molecular dynamics (MD) simulations. Compared to previous studies, our approach goes beyond two body potentials and allows the study of self-assembly starting from a completely random system, far from equilibrium, into equilibrium phases without additional assumptions, thus providing an unbiased characterization of both dynamic and static properties. Generalizations to any type of nanoparticle and/or ssDNA distribution are straightforward.

The coarse grained model is summarized in Fig. 1. The ssDNA are modeled as n_s neutral beads (the coarse grained number of spacers) and n_l number of linker beads (the coarse grained number of linkers) both of size σ. The linker beads have additional structure, model-

ing the ability to hybridize (form hydrogen bonds) complementary base-sequences. Hybridization is achieved through smaller(CT) beads with attractive interactions to their complementary (A-T,C-G). The flanking beads (FT) serve two purposes; first, forcing CT beads to interact only along the direction perpendicular to the plane tangent to the linkers, thus making the base interaction directional, as hydrogen bonds are directional. Secondly, they prevent any base from binding to more than one complementary base, an artifact that occurs for $\epsilon_{bp}/k_BT >> 1$ if FL beads are absent. The model bears some obvious resemblance with the one previously discussed by Sciortino, Starr and collaborators [14] although we find that incorporation of the FL beads is critical to ensure that artifacts such as "hybridizations" of three ssDNA or more never occur.

GNPs are built by positioning beads on a spherical surface of radius $R = 3\sigma$. ssDNAs are distributed uniformly across the GNP surface. The simulations are run using HOOMD-blue [16][17] within the NVT ensemble using the Noose-Hoover thermostat. Additionally, rigid body dynamics enforce the spherical shape of GNPs[18]. The detailed description of the model and simulation protocol can be found in the supplementary material.

The relevant parameters in the system are r, the number of ssDNA strands per GNP, and the volume fraction η, defined from the averaged end-to-end distance(T) of relaxed ssDNAs and the radius R of the GNPs (see Fig. 1).

$$\eta = \frac{N_{GNP} 4\pi (R+T)^3}{3L^3} \ , \qquad (1)$$

where N_{GNP} is the number of nanoparticles and L is the linear size of the simulation box. In converting to real units, $\sigma \sim 2$nm, $R \sim 3\sigma = 6$nm and $n_l = 3$, corresponding to ~ 20 linkers, consistent with experiments [4] as well as the measured Kuhn length for ssDNA [6]. Unless otherwise stated $N_{GNP} = 54$, and the system consists of $N_{GNP}/2$ A-GNPs and B-GNPs with A and B containing linkers with bases complementary to each other.

There are two different strategies in DNA-GNP self-assembly. The first consists of mixing two types of GNPs, each one with a complementary ssDNA strand, *direct hybridization* [4]. In the second strategy, the two types of GNPs do not have complementary ssDNA. Instead, a single ssDNA strand with complementary sequences for A and B GNPs mediates the assembly, *linker mediated hybridization* [5, 8]. For simplicity, this paper deals exclusively with the case of direct hybridization.

In Fig. 2 we show the number of hybridizations per GNP $n(H)$ as a function of temperature, where a hybridization is defined if all linkers within a strand form hydrogen bonds, i.e. are within σ of its complementary. The inset is the fraction of hybridizations $f(H)$ that live up to a time t. Reaching thermal equilibrium requires a significant number of breaking and reforming of hybridizations over the course of a simulation. The strong temperature dependence of both $n(H)$ and $f(H)$ will result in very sluggish dynamics for $T < 1.1$ and indeed, it became extremely difficult to equilibrate systems when $T < 1.1$. This strong temperature dependence has been pointed out in previous studies of micron sized particles [20] and is consistent with other studies in micellar crystals [21].

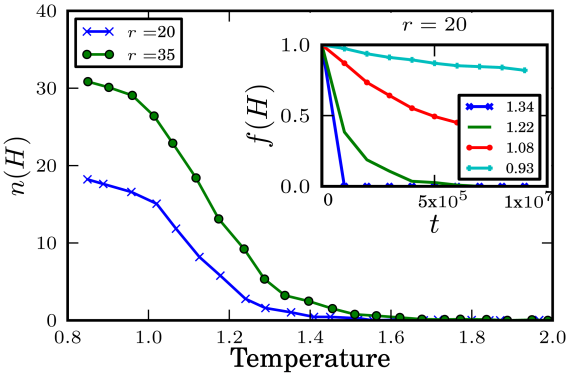

FIG. 2. (color online). Hybridizations per nanoparticle ($r = 20 - 35$, $\eta = 1.0$, $N_{GNP} = 54$) for T in $(0.8, 2.3)$. The inset shows the fraction of hybridizations that live up to a time t, $f(H)$ for different temperatures ($r = 20$).

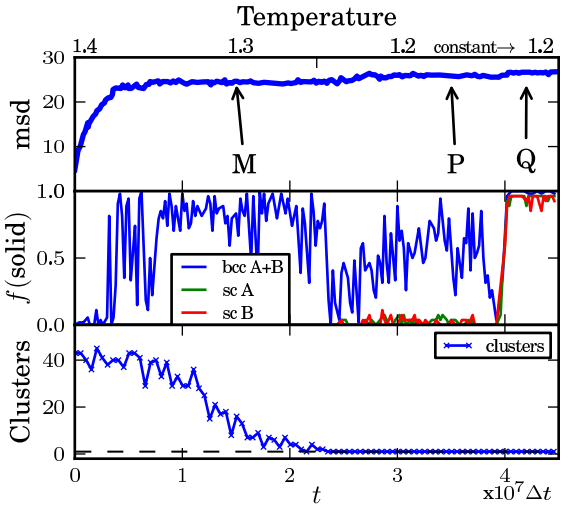

FIG. 3. (color online). Random system of GNPs at $T = 1.4$ quenched to $T = 1.2$ as a function of time. a) Mean-square-displacement. b) Fraction of solid GNPs c) Number of clusters. ($r = 25$,N$_{GNP} = 54$, $\eta = 1.0$). sc A and sc B stand for simple cubic of A,B GNPs.

A first indication of the presence of solid phases is obtained from examining the mean squared displacement (msd). As shown in Fig. 3a), a random configuration of GNPs diffuses rapidly in the early stages, gradually slowing down as particles form solid structures, as identified from the bond order parameter [22], shown in Fig. 3b). Upon further cooling, the system eventually assembles into a bcc-lattice with A and B GNPs forming a simple

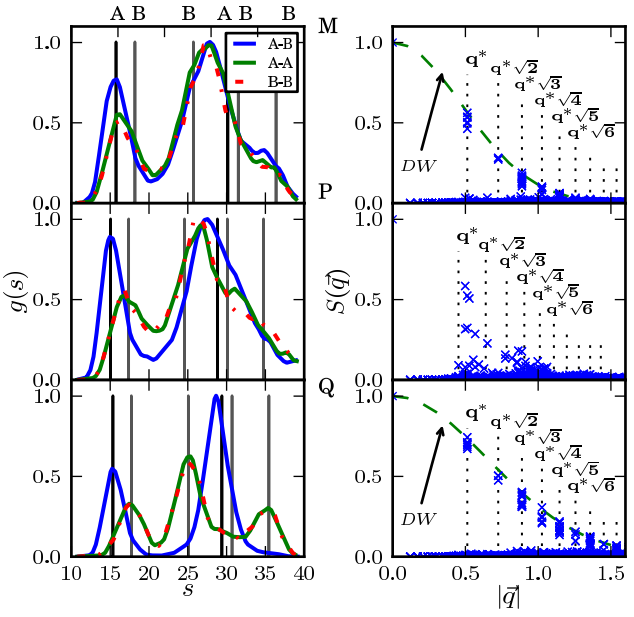

FIG. 4. (color online). Instantaneous structures of points M, P and Q in Fig. 3. (left) Pair distribution function between GNPs. The vertical lines correspond to the bcc positions $(\frac{a}{2},\frac{a}{2},\frac{a}{2}),(a,0,0),(a,a,0)$, etc. (right) Static structure factor, where dotted vertical lines correspond to the bcc lattice Bragg peaks. The Debye-Waller factor(DW) Eq. 2 is shown.

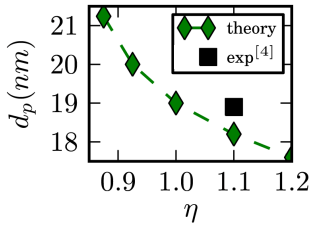

FIG. 5. (color online). Interparticle distance d_p vs η, where $d_p = a_{bcc} - 2R$. Experimental results are from Ref. [4].

cubic (sc) lattice each, the CsCl-bcc phase, at $T = 1.2$. Also plotted in c) is the number of clusters, defined as the number of disconnected networks of hybridized particles.

A detailed analysis of the structure as a function of time shows that solid particles at the higher temperatures already form a bcc lattice as shown in Fig. 4a), but the A and B GNPs are disordered (D-bcc phase). At intermediate temperatures, near $T = 1.2$ and coinciding with the formation of a single cluster connecting all GNPs (see Fig. 3), small crystallites of the CsCl-bcc phase start to nucleate and the D-bcc phase disappears (Fig. 4b), until a sharp fluctuation accompanied with a measurable diffusion of GNPs brings A and B into place and the the CsCl-bcc phase is formed, Fig. 4c and 6(b).

The phase diagram as a function of r, T and η is shown in Fig. 7. Generally, the CsCl-bcc phase is the stable one for $T < T_c(r,\eta)$ and coexists, either with D-bcc Fig. 6(a) for $r > r_M(\eta)$ or with a liquid/disordered (solid-like without Bragg peaks) for $r < r_M(\eta)$. The distinction between liquid and disordered refers to whether the diffusion coefficient of GNPs is zero. As a control simulation, the phase diagram of a system where GNP linkers are replaced by spacers ($\epsilon_{bp} = 0$), hence the GNPs become a system of f-star polymers, shows only D-bcc and liquid phases (Fig. 7). The phase diagram of f-star polymers has been characterized in Ref. [23] and it is in good agreement, see Fig. 7 (with rescaled 0.75σ). The robustness of the results against finite size effects were tested by repeating some runs in larger systems, more extensively for $N_{GNP} = 72$ and 128. Albeit with longer equilibration times and minor quantitative corrections in phase boundaries, the conclusions reported remain unchanged.

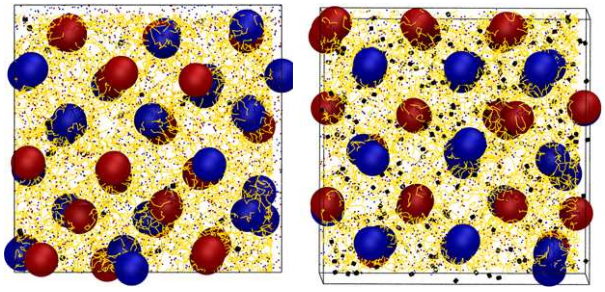

FIG. 6. (color online). Equilibrated snapshots of a) D-bcc and b) CsCl-bcc, with A (blue) and B (red) GNPs and hybridizations (black) (other colors from Fig. 1).

The simulation provides single crystals, and the form factor of single GNPs can be trivially factored out [21] from the structure factor, so the Bragg peaks at $\vec{q} = \vec{G}$ are suppressed according to the Debye-Waller factor

$$S(\vec{q} = \vec{G}) \propto \exp(-\langle \Delta r^2 \rangle |\vec{G}|^2/3), \qquad (2)$$

which provides an excellent fit to the simulation results, see Fig. 4, where $\langle \Delta r^2 \rangle^{1/2} = 0.12 a_{bcc}$. The considerable fluctuations from the perfect nearest-neighbor separation a_{bcc} is typical of self-assembled crystals [21]. Experimentally, about 14 peaks are reported, the same number we obtain, thus providing indirect evidence on the validity of the calculated Debye-waller factors.

The computed phase diagram Fig. 7 can be compared with experiments [8] with some caveats as the latter correspond to linker mediated with varying linker lengths. Upon correcting for linker concentration by shifting η, results show good agreement. The interparticle distance $d_p = a_{bcc} - 2R$ (thus defined to emphasize ssDNA conformation) shown in Fig. 5 as a function of η, in agreement with experimental results for direct hybridization [4].

The D-bcc phase is crystalline, as evidenced from the Bragg peaks in Fig. 4, and the transition from D-bcc to CsCl-bcc is expected to be first order as evidenced from the nucleation and growth plots in Fig. 3. The reason why the D-bcc phase has not been reported experimentally is that A-GNPs and B-GNPs are indistinguishable in SAXS. Other experiments, not performed to date, such as SANS with deuterated ssDNAs as well as calorimetric

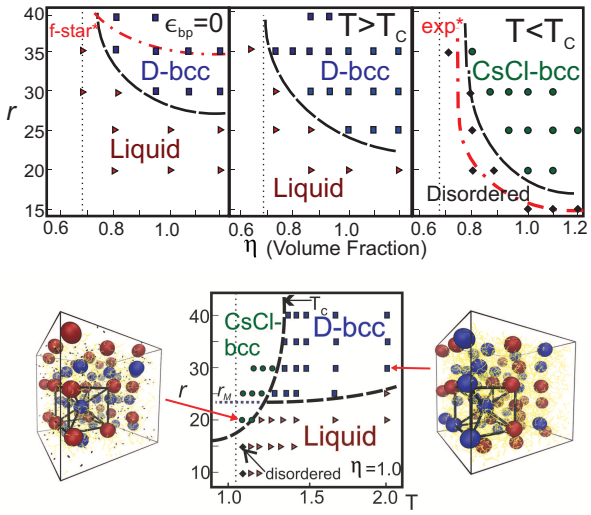

FIG. 7. (color online). Top: phase diagram r vs. η for $\varepsilon_{bp} = 0$ (f-star polymers) and $\varepsilon_{bp} = 10$. The dotted line on the left is the location of bcc for hard spheres. Bottom: phase diagram for r vs temperature ($\eta = 1.0$). Phase boundaries are approximate. The f-star are from [23] and the experimental line from [8], shifted as discussed in the text. Snapshots include the reconstructed bcc lattice from the $S(\vec{q})$.

or rheological measurements should be able to establish the D-bcc phase. We note that for linker mediated hybridization, the linkers at larger temperatures behave as homopolymers, thus providing f-star polymers with the ability to diffuse leading to the destabilization of the D-bcc phase.

In summary, we establish that the dynamics of CsCl-bcc proceeds first by forming a single cluster where all GNPs are connected by hybridization. This large cluster consists of only a fraction of particles in a solid phase with Bragg peaks, but without any obvious structure, see Fig. 4 at P. Within this intermediate state, small-sized crystallites of short-lived CsCl-bcc nucleate until a sharp fluctuation accompanied with significant GNP diffusion reaches the critical nucleus leading to the CsCl-bcc phase. Given the strong temperature dependence of the interactions as well as diffusion coefficients as a function of r, relaxation times for $T << T_c$ and $r \geq 35$, quickly become of the order of the simulation (or experimental) time and metastable crystalline states such as in Fig. 4P, may show up as stable, a result also reported experimentally[4, 5].

Furthermore, we have shown that the coarse-grained model described in Fig. 1 is able to account for existing experimental results and contains a number of new testable predictions, both in regards to dynamics and statics. The main limitation in our study is the relatively small number of GNPs (up to 128) considered, and the range of temperatures. Larger number of GNPs may be relevant to establish the real size of the critical nucleus, but demands the use of more sophisticated methods, most promisingly parallel tempering [24]. Yet, as discussed, it is expected to affect quantitative aspects only. How to extend DNA programmable self-assembly to predict the rich phases found in closely related systems [11] will be the subject of future studies.

Acknowledgments We acknowledge discussions with J. Anderson, O. Gang, D. Nykypanchuk and C. Philips. S.B acknowledges a DOE SULI internship at the Ames Lab. This work is funded by DOE through the Ames Lab under Contract DE-AC02-07CH11358.

[1] C. Mirkin, R. Letsinger, R. Mucic and J. Storhoff, *Nature* **382** 607 (1996).
[2] A. Alivisatos et al. *Nature* **382** 609 (1996).
[3] M. Valignat et al., *PNAS* **102**, 4225 (2005); M. Leunissen et al., *Nature Mater.* **8**, 590 (2009). A.J. Kim et al., *Nature Mater.* **8**, 52 (2009).
[4] D. Nykypanchuk, M. Maye, D. van der Lelie and O. Gang *Nature* **451** 549 (2008).
[5] S.Y. Park et al., *Nature* **451** 553 (2008).
[6] K. Rechendorff, G. Witz, J. Adamcik and G. Dietlera *J. Chem. Phys.***131** 095103 (2009).
[7] H. Hill et al., *Nano Lett.* **8** 2341 (2008).
[8] H. Xiong, D. van der Lelie and O. Gang, *Phys. Rev. Lett.* **102** 015504 (2009).
[9] M. Maye et al., *Nature Nanotechnology* **5** 116 (2010).
[10] K. Suzuki, K. Hosokawa and M. Maeda, *JACS* **131** 7518 (2009).
[11] C. Knorowski, J. Anderson and A. Travesset, *J. Chem. Phys.* **128** 164903 (2008); R. Sknepnek et al., *ACS nano* **2** 1259 (2008); J. Anderson, R. Sknepnek and A. Travesset, *Phys. Rev. E* **82** 021803 (2010).
[12] A. Tkachenko, *Phys. Rev. Lett.* **89** 148303 (2002).
[13] D. Lukatsky, B. Muller and D. Frenkel, *J. Phys. Condens. Matt.* **18** S567 (2006).
[14] J. Largo, F. Starr and F. Sciortino, *Langmuir* **23** 5896 (2007); W. Dai, C. Wei Hsu, F. Sciortino and F. Starr, *Langmuir* **26** 3601 (2010).
[15] R.T. Scarlett, M. Ung, J. Crocker and T. Sinno, *Soft Matter* **advanced article** (2011).
[16] J. Anderson, C. Lorenz and A. Travesset, *J. Comput. Science* **227** 5342 (2008).
[17] **http://codeblue.umich.edu/hoomd-blue/**.
[18] T. Nguyen, C. Philips, J. Anderson and S. Glotzer, *preprint submitted* (2011).
[19] L. Martinez, R. Andrade, E. G. Birgin and J. M. Martinez, *J. Comput. Chem.* **30(13)** 2157 (2009).
[20] P. Biancanello, A. Kim and J. Crocker, *Phys. Rev. Lett.* **94** 058302 (2005).
[21] J. Anderson, C. Lorenz and A. Travesset, *J. Chem. Phys.* **128** 184906 (2008).
[22] P. Steinhardt, D. Nelson and M. Ronchetti, *Phys. Rev. B* **28** 784 (1983).
[23] M. Watzlawek, C. Likos and H. Lowen, *Phys. Rev. Lett.* **82** 5289 (1999).

[24] D. Earl and M. Deem, *Phys. Chem. Chem. Phys.* **7** 3910 (2005).